

# How Hydrogen Bonds Influence the Mobility of Imidazolium-Based Ionic Liquids. A Combined Theoretical and Experimental Study of 1-*n*-Butyl-3-methylimidazolium Bromide

Miriam Kohagen,<sup>†</sup> Martin Brehm,<sup>†</sup> Yves Lingscheid,<sup>‡</sup> Ralf Giernoth,<sup>‡</sup> Joshua Sangoro,<sup>§</sup> Friedrich Kremer,<sup>§</sup> Sergej Naumov,<sup>§</sup> Ciprian Iacob,<sup>§</sup> Jörg Kärger,<sup>§</sup> Rustem Valiullin,<sup>§</sup> and Barbara Kirchner<sup>\*,†</sup>

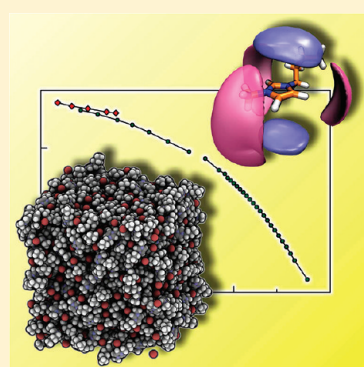
<sup>†</sup>Wilhelm-Ostwald-Institut für Physikalische und Theoretische Chemie, Universität Leipzig, Linnéstr. 2, D-04103 Leipzig, Germany

<sup>‡</sup>Department für Chemie der Universität zu Köln, Greinstr. 4, D-50939 Köln, Germany

<sup>§</sup>Institut für Experimentelle Physik I, Universität Leipzig, Linnéstr. 5, D-04103 Leipzig, Germany

**S** Supporting Information

**ABSTRACT:** The virtual laboratory allows for computer experiments that are not accessible via real experiments. In this work, three previously obtained charge sets were employed to study the influence of hydrogen bonding on imidazolium-based ionic liquids in molecular dynamics simulations. One set provides diffusion coefficients in agreement with the experiment and is therefore a good model for real-world systems. Comparison with the other sets indicates hydrogen bonding to influence structure and dynamics differently. Furthermore, in one case the total charge was increased and in another decreased by 0.1 e. Both the most acidic proton as well as the corresponding carbon atom were artificially set to zero, sequentially and simultaneously. In the final setup a negative charge was placed on the proton in order to introduce a barrier for the anion to contact the cation via this most acidic hydrogen atom. The following observations were made: changing the hydrogen bonding ability strongly influences the structure while the dynamic properties, such as diffusion and viscosity, are only weakly changed. However, the introduction of larger alterations (stronger hydrogen bonding and antihydrogen bonding) also strongly influences the diffusion coefficients. The dynamics of the hydrogen bond, ion pairing, and the ion cage are all affected by the level of hydrogen bonding. A change in total charges predominantly influences transport properties rather than structure. For ion cage dynamics with respect to transport properties, we find a good correlation and a weak or no correlation for the ion pair or the hydrogen bond dynamics, respectively. Nevertheless, the hydrogen bond does influence ion cage dynamics. Therefore, we confirm that ionic liquids rather consist of loosely interacting counterions than of discrete ion pairs. Hydrogen bonding affects the properties only in a secondary or indirect manner.



## INTRODUCTION

Hydrogen bonding in imidazolium-based ionic liquids is a highly controversial issue.<sup>1–9</sup> Ionic liquids—being liquid substances composed entirely of ions—still show many unexplained phenomena.<sup>10</sup> In some investigations, hydrogen bonding seems to be important, in others not.<sup>11,12</sup> It sometimes enhances certain transport properties but opposite effects have also been reported.<sup>2,3,7,13</sup> One example is the increase of viscosity (melting point) when hydrogen bonding is eliminated by replacing the acidic proton in imidazolium-based ionic liquids with a methyl group.<sup>14,15</sup> Nishikawa and co-workers could show by NMR spectroscopy that the origin of this effect does not stem from the reduction of butyl group motion but from the amount of stable anion interaction sites.<sup>16,17</sup> Additionally, it is suggested that viscosity increase by C(2) methylation can be interpreted accordingly. In contrast, lower viscosities were observed in acidic AlCl<sub>3</sub> melts where larger anions give rise to lower hydrogen bonding.<sup>2</sup>

Previously, as an experiment in the virtual laboratory, we explored the tremendous influence of different quantum

chemically derived charges applied in molecular dynamics simulations on structural properties, i.e., in computer simulations.<sup>18</sup> The system under investigation in both studies is the ionic liquid 1-*n*-butyl-3-methylimidazolium bromide ([C<sub>4</sub>C<sub>1</sub>im][Br]). While two models (natural bond orbital (NBO)<sup>19</sup> and restraint electrostatic potential (RESP)<sup>20</sup>) agree well, the third set of charges (shared electron number (SEN)<sup>21</sup>) provided erroneous results with respect to the experimentally<sup>4,22–24</sup> as well as theoretically<sup>25</sup> expected structure (cf. Figure 1 in which the spatial distribution functions are displayed<sup>18</sup>).

In this article we focus on the dynamic properties of the different charge sets. We will provide further systematically altered charge sets in order to explore the influence of hydrogen bonding. We will also prove the validity of the charge set that is usually applied in simulations<sup>18</sup> by comparing it to experiment. In

**Received:** July 21, 2011

**Revised:** November 9, 2011

**Published:** November 14, 2011

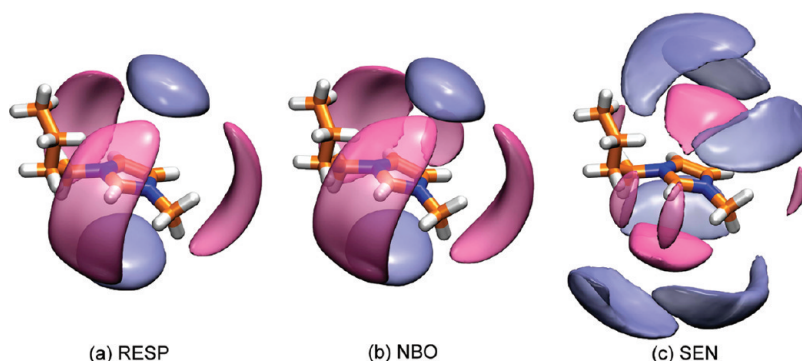


**Figure 1.** Spatial distribution of the anion around the cation in the RESP (a), NBO (b), and SEN (c) systems. The pink spheres indicate anion coordination around the cation while the blue ones mark the next cation neighbors.<sup>18</sup>

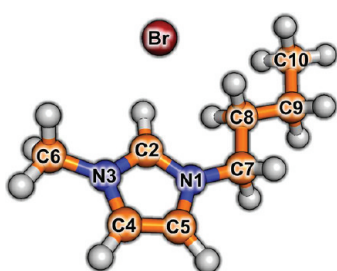


**Figure 2.** Atom labeling for  $[\text{C}_4\text{C}_1\text{im}][\text{Br}]$  as applied throughout this work.

the following, we give the computational and experimental methodologies and a description of the altered partial charges on the atoms. Finally, we provide the structural as well as the dynamic results of the simulations and discuss them.

## COMPUTATIONAL AND EXPERIMENTAL METHODOLOGIES

**Computational Details.** A detailed description of the computational methodology can be found elsewhere.<sup>18</sup> For better comparison with experiments, some additional simulations for the RESP system at different temperatures were carried out. The experiments were conducted at different temperatures  $T$ ; therefore, 360, 402, 431, and 460 K were selected as additional simulation temperatures. In this case, for all simulations an equilibration for 2 ns with the Berendsen thermostat and the Berendsen barostat<sup>26</sup> at 1 bar were performed. The coupling times of the thermostat and the barostat were 0.1 and 0.5 ps, respectively. For each temperature, two different trajectories were calculated, one with a length of 20 ns and every 5000th step stored, and one with a length of 500 ps and every 25th step stored.

For the calculation of the diffusion coefficients as well as for the viscosities we used the tools of the GROMACS 4.0.5 program package.<sup>27</sup> Every other quantity was evaluated using the program package TRAVIS.<sup>28</sup> The relaxation times  $\tau$  were calculated for the time correlation functions of hydrogen bond (HB), ion pair (IP and IP'), and ion cage (ICage) dynamics; IP is with respect to the ring center and IP' to the center of mass of the cation. For further details see Supporting Information.

**Synthesis of  $[\text{C}_4\text{C}_1\text{im}][\text{Br}]$ .**  $[\text{C}_4\text{C}_1\text{im}][\text{Br}]$  was synthesized via metathesis reaction of 1-methylimidazole with 1-butyl bromide. Therefore, 97.5 mL (903.3 mmol) of 1-butyl bromide was heated

to 70 °C and subsequently 60.0 mL (752.7 mmol) of methylimidazole was added within 2 h. The crude product was received after 2 h of additional stirring as yellow oily liquid. Via recrystallization from ice-cold ethyl acetate, 115.3 g (526.2 mmol, 70%) of the product was obtained as a white solid. After additional washing with ethyl acetate, the solid was dried in vacuo under persistent stirring. The water content was below 20 ppm (determined by Karl Fischer titration). The NMR measurements were performed in deuterated dimethyl sulfoxide ( $\text{DMSO}-d_6$ ).

$^1\text{H}$  NMR ( $\text{DMSO}-d_6$ , 400 MHz)  $\delta$  (ppm) = 9.23 (s, br, 1H, CH, H2), 7.81–7.80 (s, 1H, H4/H5), 4.18 (t, 2H,  $J$  = 7.34 Hz, H7/H7'), 3.86 (s, 3H, H6/H6'/H6''), 1.81–1.71 (quint, 2H,  $J$  = 7.42 Hz, H8/H8'), 1.285 (sext, 2H,  $^3J$  = 7.5 Hz, H9/H9'), 0.92 (t, 3H,  $J$  = 7.39, H10/H10'/H10'').

$^{13}\text{C}$  NMR ( $\text{DMSO}-d_6$ , 75 MHz)  $\delta$  (ppm) = 136.8 (s, C9), 122.4 (s, C5), 122.3 (s, C4), 48.5 (s, C7), 35.7 (s, C6), 31.4 (s, C8), 18.9 (s, C9), 13.4 (s, C10).

IR (ATR)  $\nu$  = 2963 (m), 1568 (m), 1558 (m), 1456 (w), 1163 (s), 893 (w), 810 (m), 656 (m), 631 (m).

**Pulsed Field Gradient NMR and Broad Band Spectroscopy.** The diffusion coefficients were determined experimentally using two independent measurement techniques, pulsed field gradient nuclear magnetic resonance (PFG NMR)<sup>29–31</sup> and broadband dielectric spectroscopy (BDS).<sup>32</sup> Recently, it has been demonstrated that the diffusion coefficient can be determined from BDS spectra by a combination of the Einstein and Einstein–Smoluchowski equations. Within this framework, the direct current conductivity  $\sigma_0$  is given by

$$\sigma_0 = nq\mu = \frac{nq^2}{kT} D = \frac{nq^2}{kT} \frac{\lambda^2 \omega_c}{2} \quad (1)$$

where  $n$  denotes the effective number density (given by  $N\gamma(T)$ , where  $\gamma(T)$  is the fraction of mobile charge carriers at a given temperature  $T$  and  $N$  is the total number density of charge carriers available in the material),  $\mu$  is the mobility of charge carriers,  $q$  is the elementary electric charge,  $D$  is the diffusion coefficient,  $k$  is the Boltzmann constant,  $\lambda$  denotes the hopping length, and  $\omega_c$  is the characteristic (diffusion) rate. Rearranging the eq 1 leads to an expression for the diffusion coefficient  $D$ :

$$D = \frac{\lambda^2 \omega_c}{2} \quad (2)$$

Further details can be found in our previous work and in textbooks.<sup>29,32</sup>

**Table 1.** Comparison of the Charges  $q$  for the Carbon and Hydrogen Atoms of the Imidazolium Ring<sup>a</sup>

	$q(\text{C2})$	$q(\text{H2})$	$q(\Sigma 2)$	$q(\text{C4})$	$q(\text{H4})$	$q(\Sigma 4)$	$q(\text{C5})$	$q(\text{H5})$	$q(\Sigma 5)$	$q(\text{Br})$
RESP	0.00	0.19	0.19	−0.12	0.19	0.07	−0.19	0.21	0.02	−0.80
NBO	0.29	0.25	0.54	−0.01	0.26	0.25	−0.03	0.23	0.20	−0.85
SEN	0.06	0.04	0.10	0.06	0.03	0.09	0.04	0.00	0.04	−0.89
0.7	0.00	0.16	0.16	−0.11	0.17	0.06	−0.16	0.19	0.03	−0.70
0.9	0.00	0.21	0.21	−0.14	0.21	0.07	−0.21	0.24	0.03	−0.90
$\text{H2}^0\text{C2}^0$	0.00	0.00	0.00	−0.11	0.21	0.10	−0.17	0.24	0.07	−0.80
$\text{H2}^0\text{C2}^{0.19}$	0.19	0.00	0.19	−0.12	0.19	0.07	−0.19	0.21	0.02	−0.80
$\text{H2}^{-0.19}\text{C2}^0$	0.00	−0.19	−0.19	−0.10	0.24	0.14	−0.15	0.27	0.12	−0.80

<sup>a</sup> Charges in e (atomic units). (2 marks the most acidic position and 4 as well as 5 label the remaining positions on the rear.) For labeling, see Figure 2 in the Computational and Experimental Methodologies section.

## ■ CHARGE SETUP

In the introductory section, the diverging structures resulting from previously applied charge sets were depicted. The question arises as to whether we can relate the virtual experiment to a physically meaningful picture. Here, we concentrate on the particular atomic charges. The first three entries of Table 1 show the differences induced by different quantum chemically derived charge sets.

While for the hydrogen atom the charges between RESP and NBO resemble each other best, the group charges  $q(\Sigma)$  calculated by adding up the values of carbon and hydrogen atom agree better between RESP and SEN. For the  $q(\text{H2})$  and the  $q(\Sigma 2)$  values the order is SEN, RESP, and NBO, starting from the smallest value. Physically, this means that the hydrogen-bonding ability for the NBO charges is enhanced, whereas the acidity is decreased in the SEN system. Furthermore, the charges are distributed more on the surface of the cation in the NBO calculations than in the other ones, because the terminal atoms possess higher charges in the NBO analysis.

Previously, Youngs and Hardacre thoroughly investigated the effect of changing the total charges on the ions.<sup>33</sup> Therefore, we added only two experiments in which we up-scaled and down-scaled the total RESP charges by 0.1 e on the ions (see entries 4 and 5 in Table 1). This alteration of the total charges leads to almost no change of the individual charges on the hydrogen atoms.

Table 1 also contains artificially altered atomic charges (shown in the last three entries). For these setups the total charges remain constant, but the individual charges at the most acidic group are manipulated. The set denoted  $\text{H2}^0\text{C2}^0$  holds on both C2 and H2 zero charge, the set  $\text{H2}^0\text{C2}^{0.19}$  shifts the charge of the proton onto the carbon atom, and in the last setup  $\text{H2}^{-0.19}\text{C2}^0$  we altered the sign of the H2 charge. The total charges are held constant by distributing the remainder equally on all other atoms. Physically, this means that the already weak hydrogen bond ability of C2–H2 is neutralized in  $\text{H2}^0\text{C2}^0$  and it is eliminated in  $\text{H2}^0\text{C2}^{0.19}$ , because this system is unable to let the proton act as the hydrogen bridge toward the anion; i.e., the attraction is now provided from the carbon atom only. The  $\text{H2}^{-0.19}\text{C2}^0$  introduces a barrier for the anion to approach the cation via the C2–H2 group, because the proton now bears a negative charge. In the following we will call this scenario “anti-hydrogen bonding” (due to the opposite sign of the charges compared to that of a conventional hydrogen bond).

## ■ STRUCTURE

For the structural properties, it seems to be more important to have similar charges on the hydrogen atoms than similar group charges, which was shown in our previous publication (see also

Figure 1).<sup>18</sup> A slight increase of the hydrogen bonding, reflected in high  $q(\text{H2})$  values at the NBO set, does not change the structure much while a large decrease of the hydrogen bonding alters the results tremendously. Contrary to that, similar  $q(\Sigma)$  do not lead to the same structure when the individual contributions on C and H are very different.<sup>18</sup>

In Figure 3 we compare the new setups with altered total charges.

The changes according to total charges are only marginal, as previously observed and discussed by Youngs and Hardacre:<sup>33</sup> “[...] Nevertheless, fairly large deviations from the original set of charges are required to promote these effects—for small deviations the macroscopic features of the liquid structure are maintained. [...]” These “large deviations” in order to change the structural features are a total charge change of more than 0.4 e.<sup>33</sup>

The results of the altered C2–H2 charges at constant total charges are more exciting. These are depicted in Figure 4.

Neutralization of the charge ( $\text{H2}^0\text{C2}^0$ ) on the hydrogen atom leads to a shift of the anion coordination from H2 toward the methyl group and an increased occupation of the rear hydrogen atoms H4 and H5 (Figure 4b). Please note that some “hydrogen-bond-like” conformations are still recognizable. The next neighbor cations (blue spheres) are still able to approach the observed cation from above and below the imidazolium ring in order to promote Lennard-Jones contacts. Shifting the charge from the hydrogen atom to the C2 atom ( $\text{H2}^0\text{C2}^{0.19}$ ) destroys the hydrogen bond which is reflected in the “hole” in the pink sphere at the C2–H2 group (Figure 4c). Furthermore, small probabilities of next cation coordination to the observed cation via H2 are visible by the small blue sphere in front of H2. However, the dominant approach of the next cationic neighbor still seems to appear from above and below the imidazolium ring. For the third charge setup ( $\text{H2}^{-0.19}\text{C2}^0$ ), this observation is much extended, since now a large blue sphere is reaching from below via H2 to above the ring plane for the next cation neighbors (Figure 4d). Anion coordination now solely proceeds via the rear positions and the methyl group. This is in accordance with observations by the Seddon group for a methylated imidazolium-based ionic liquid. The authors found structures in which cations closely approach each other.<sup>1</sup> Replacement of the hydrogen with a methyl group at the C2 position is known to hinder approach of the anion to this region of the imidazolium ring.<sup>6,14</sup> This seems to indicate that we can compare our antihydrogen bond situation to a methyl substitution at the most acidic ring proton.

## ■ TRANSPORT PROPERTIES AND COHESIVE ENERGY

The picture changes when considering dynamical properties. In the previously obtained charge sets, the third one (SEN)



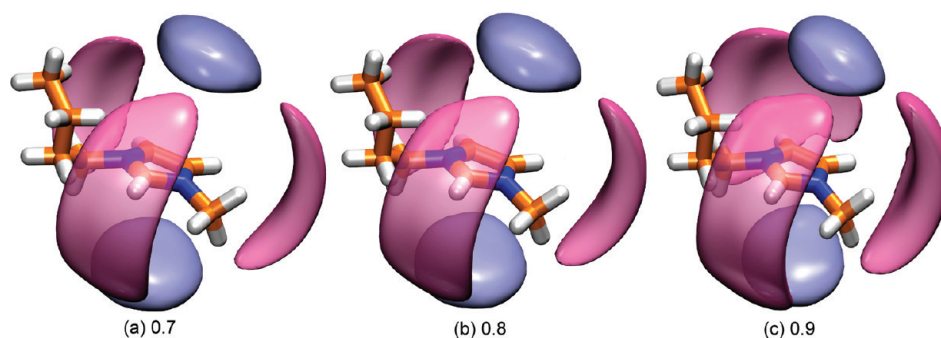


**Figure 3.** Spatial distribution of the anion around the cation. The pink spheres indicate anion coordination around the cation while the blue ones mark the next cation neighbors. Displayed is the original RESP (a) system and the two setups with up-scaled (b) and down-scaled (c) total charge.

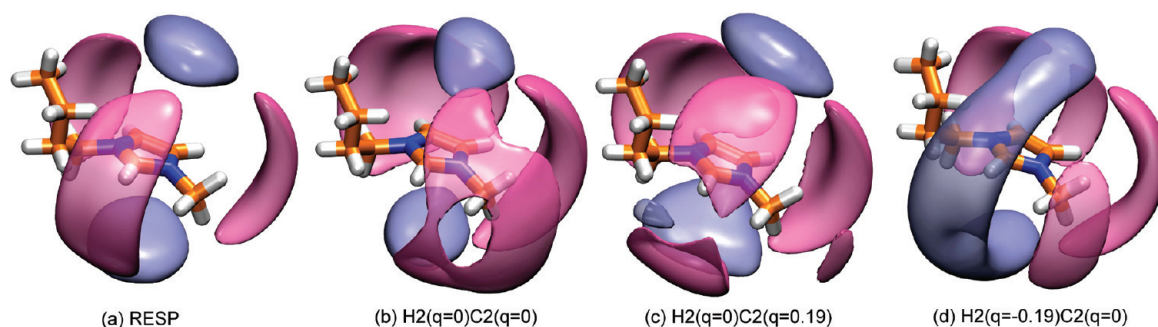


**Figure 4.** Spatial distribution of the anion around the cation. The pink spheres indicate anion coordination around the cation while the blue ones mark the next cation neighbors. Displayed is the original RESP (a) system, and the three setups with altered C2–H2 charges (b,c,d).

**Table 2.** Diffusion Coefficients Calculated for the RESP System at Different Temperatures (First Block) and for the Different Charges at 373 K (Second Block) Using the Einstein and Green–Kubo Relations<sup>a</sup>

	Einstein		Green–Kubo		$U_{\text{liq}}$
	$[\text{C}_4\text{C}_{1\text{im}}]^+$	$[\text{Br}]^-$	$[\text{C}_4\text{C}_{1\text{im}}]^+$	$[\text{Br}]^-$	
360 K	0.22	0.21	0.27	0.25	−202
373 K	0.28	0.26	0.32	0.29	−201
402 K	0.51	0.50	0.54	0.48	−197
431 K	0.75	0.71	0.81	0.72	−195
460 K	1.29	1.31	1.14	1.21	−190
373 K					
RESP	0.28	0.26	0.32	0.29	−201
NBO	0.03	0.03	0.06	0.05	—
SEN	0.14	0.15	0.15	0.20	−380
0.7	0.71	0.69	0.81	0.78	−158
0.9	0.09	0.08	0.10	0.09	−251
$\text{H}_2^0\text{C}_2^0$	0.32	0.30	0.36	0.33	−233
$\text{H}_2^0\text{C}_2^{0.19}$	0.32	0.26	0.35	0.28	−257
$\text{H}_2^{-0.19}\text{C}_2^0$	0.06	0.07	0.11	0.14	−304

<sup>a</sup> All values are in  $10^{-5} \text{ cm}^2/\text{s}$ . Errors are discussed in the Supporting Information. The cohesive energy per ion pair  $U_{\text{liq}}$  is given in kJ/mol. An explanation for the missing value (NBO) is given in the text.

comes close to the results from the experimentally adjusted charge set (RESP) (Table 2). Some diffusion coefficients calculated using the Einstein relation and the Green–Kubo relation

are also given in Table 2. In order to obtain well-sampled results, we analyzed the 20 ns long trajectories utilizing the Einstein relation. The results from the Green–Kubo relation were obtained from the first 100 ps of the trajectories with a length of 500 ps and a time step of 0.001 ps. For details see Supporting Information.

The diffusion coefficients from both relations are of the same order of magnitude. The coefficients increase with increasing temperature which means more diffusive motion. For the anion, slightly smaller values are obtained than for the cation in almost all cases—a phenomenon that has been observed and discussed before.<sup>34,35</sup>

In Figure 5 the experimental data from pulsed field gradient NMR (PFG NMR) and broadband dielectric spectroscopy (BDS) measurements indicated by open symbols and the theoretical values from the RESP simulation denoted by the filled symbols are shown. The values from the RESP simulations fit the Vogel–Fulcher–Tammann equation in the entire calculated temperature range well. The agreement with the experimental values is reasonable in the overlap region between 358 and 415 K. To improve the agreement between experiment and calculations, one could use polarizable force fields. This was shown by Yan et al.<sup>37</sup> In the framework of our simulations, we can conclude that the RESP system covers the experimentally expected picture best and is therefore used as reference system. Turning now to it again, we observe an interesting result. Surprisingly, for both ions, the highest diffusion coefficients can be observed in the RESP system followed by the SEN system and the lowest in the NBO system. The diffusion coefficients for the calculations using SEN charges are about 2–3 times the values from the simulations

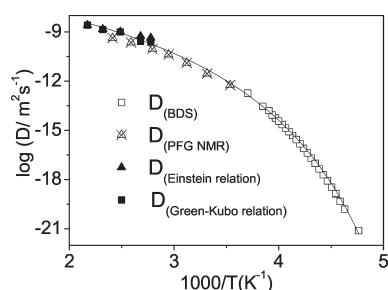


**Figure 5.** Diffusion coefficients from dielectric spectra (BDS) for  $[C_4C_{1im}][Br]$  (empty squares) and from PFG NMR (crossed triangles). Theoretical values from Einstein and Green–Kubo relations for  $[C_4C_{1im}][Br]$  are indicated by filled squares and triangles, respectively. The line denotes a fit by the empirical Vogel–Fulcher–Tammann equation.<sup>36</sup>

using NBO charges and half as large as the ones from the RESP trajectory. This is not understandable from the charges on the hydrogen atoms, since the RESP set possesses a large charge on H2 ( $q = 0.19$  e) and SEN a small ( $q = 0.04$  e). If this would be the only crucial size, one would expect that the SEN system has a faster dynamics than the RESP system. Another crucial size could be the total charges which are largest in the SEN system. Therefore, one would expect SEN to be slower than RESP and NBO, which it is not the case. Thus, if only the hydrogen bonding would affect the mobility, the diffusion coefficient should increase (decrease) in case of lower (higher) hydrogen bonding strength which is again reflected in lower (higher) positive charges on the hydrogen atoms. If only the total charges of the ions would affect the diffusion coefficients, a higher total charge would result in a lower diffusion coefficient and vice versa. However, both effects together (no hydrogen bonding and highest total charge) as they occur in the SEN system might lead to a net effect of mobility lying in between the strong (NBO) and the normal (RESP) hydrogen-bonding ability. Therefore, the mobility seems to be influenced by both the hydrogen bonding as well as the pure Coulombic forces.

In order to reveal the individual contributions, we checked the outcome of our artificially altered charge systems. The sets with altered total charge in Table 2 confirm the intuitive picture: larger total charges result in smaller diffusion coefficients, i.e., slower diffusive motion and vice versa, which has been observed by Youngs and Hardacre before.<sup>33</sup> Interestingly, the neutralization of the hydrogen bond increases the motion slightly, but only small changes are visible compared to the RESP system. However, this is not the case for the  $H2^{-0.19}C2^0$  set. Clearly, this extreme non-hydrogen-bond situation results in the opposite trend that was observed for the neutralized hydrogen-bonded system  $H2^0C2^0$  or the inverse charge set system  $H2^0C2^{0.19}$ : the diffusion coefficients decrease. For these last three charge sets, the total charges were kept constant.

This leads to the general conclusion that totally altered charges do influence the diffusive motion. Also, strong changes in hydrogen bonding, as reflected in the NBO and the  $H2^{-0.19}C2^0$  charge sets, influence diffusion.

The cohesive energy as discussed by Lynden-Bell and Youngs is calculated as the total intermolecular potential energy divided by the number of ion pairs. Physically, this gives the solvent effect, i.e., the energy of the separated ions in the gas phase minus the energy of the liquid phase.<sup>35</sup> Parallel trends are observed with diffusion coefficients. Such a correlation between diffusion and

**Table 3.** Viscosities<sup>a</sup>

$\eta$	
373 K	
RESP	1.42
NBO	2.45
SEN	1.73
0.7	0.92
0.9	2.00
$H2^0C2^0$	1.36
$H2^0C2^{0.19}$	1.40
$H2^{-0.19}C2^0$	2.08

<sup>a</sup> All values are in  $10^{-3}$  kg/(m·s), and errors are discussed in the Supporting Information.

effective cohesive energy was previously observed by Borodin.<sup>38</sup> In our investigation this trend can clearly be seen in the temperature-dependent data set (Table 2, first block) and for the altered total charges. The NBO system does not fit the trend at all—it has an unreasonable high cohesive energy with respect to its low diffusion coefficient. Therefore, the value is omitted in Table 2. An explanation might be that the high total charges on the atoms affect the calculation of the long-range electrostatic energies which are part of the cohesive energy.

Estimates of the viscosities were obtained via the transverse-current autocorrelation function.<sup>27</sup> Please note that these values have to be treated with care, for the calculation of viscosities is a nontrivial task; see ref 39 for further information. For a discussion regarding the problems of our analysis, see the Supporting Information. The RESP results for the different temperatures (360 K,  $(1.49 \pm 0.08) \times 10^{-3}$  kg/(m·s); 373 K,  $(1.42 \pm 0.08) \times 10^{-3}$  kg/(m·s); 402 K,  $(1.28 \pm 0.09) \times 10^{-3}$  kg/(m·s); 431 K,  $(1.03 \pm 0.05) \times 10^{-3}$  kg/(m·s); 460 K,  $(0.90 \pm 0.04) \times 10^{-3}$  kg/(m·s)) follow the expected trend: the viscosities decrease with increasing temperature.

The highest viscosity can be observed in the NBO system and the smallest in the RESP system (Table 3) which parallels the trends from diffusion. Again, the RESP and the SEN results are much closer together. Thus, reducing the hydrogen bonding hardly affects viscosity, but strengthening hydrogen bonding has a strong influence. Also, it is surprising that the reduction of the hydrogen-bonding ability as provided in the  $H2^{-0.19}C2^0$  simulations leads to an increase of viscosity instead of a decrease. However, this is exactly observed when a barrier is introduced via methyl substitution instead of eliminating the hydrogen bond interaction: the viscosity of the methylated substance becomes larger.<sup>2,14,15</sup> The other charge sets as well confirm the trend of the diffusion coefficients.

An experimental value for the viscosity was measured to be 1.486 kg/(m·s) at 298 K.<sup>40</sup> Another literature value is given with 1.514 kg/(m·s) at 294 K.<sup>41</sup> The water content of the measurements in  $[C_4C_{1im}][Br]$  was 1.8 wt % which changes the outcome largely. The presence of small amounts of water or other impurities such as chloride are known to remarkably influence the viscosity of ionic liquids.<sup>42</sup> Although the latter has to be treated with care, this is one reason for the discrepancy between these experimental values and the calculated results. Furthermore, viscosities between  $5 \times 10^{-3}$  and  $15 \times 10^{-3}$  kg/(m·s) at 373 K and between  $5 \times 10^{-3}$  and  $20 \times 10^{-3}$  kg/(m·s) in a temperature range between 363 and 393 K are generally calculated<sup>42</sup> which is of same order of magnitude as our results.

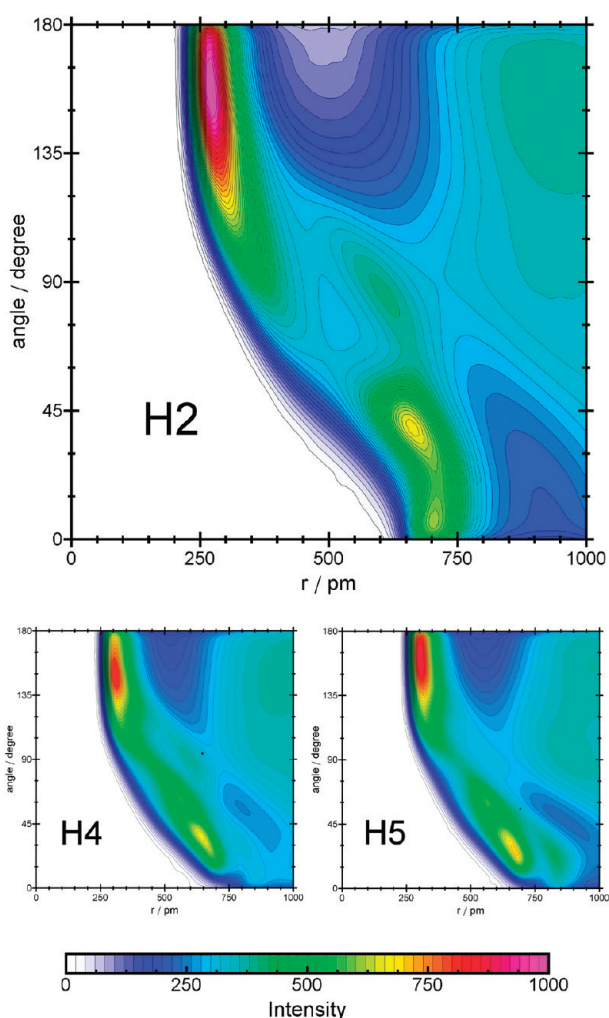


**Figure 6.** Combined distribution function build from HX–Br distance ( $X = 2, 4$ , and  $5$ ;  $x$ -axis) and angle between the HX–CX and HX–Br vectors ( $y$ -axis). The red color indicates high geometric probabilities changing from yellow via green to blue which illustrates lower probabilities.

## ■ HYDROGEN BOND AND ION PAIR DYNAMICS REVISITED

In order to analyze the hydrogen bond dynamics and set a reasonable hydrogen bond criterion, we show in Figure 6 the combined distribution function of the HX–Br distance and the CX–HX–Br angle.

There are two distinct coordination sites of the anion toward the ring hydrogen atoms of the cation. For each ring hydrogen atom there is one peak at  $>250$  pm (HX–Br distance) and  $90$ – $180^\circ$  (CX–HX–Br angle) and another one around  $<750$  pm and  $0$ – $45^\circ$ , respectively. While the first peak is the H–Br coordination of the particular hydrogen, the latter is due to the two other ring hydrogen atoms. It is apparent from Figure 6 that a traditional hydrogen bond criterion applying the first minimum (ca.  $500$  pm) of the radial pair distribution function and  $130$ – $180^\circ$  is not sufficient to describe the location of high probabilities. According to Figure 6 we rather use angles between  $120^\circ$  and  $180^\circ$  and distances smaller than  $375$  pm in order to set a hydrogen bond criterion for this particular liquid. A more extended discussion is given elsewhere.<sup>28</sup>

**Table 4.** Relaxation Times  $\tau$  from Time Correlation Functions of Hydrogen Bonds (HB), Ion Pairs (IP and IP'), and Ion Cages (ICage)<sup>a</sup>

	$\tau_C^{\text{HB/H5}}$	$\tau_C^{\text{HB/H4}}$	$\tau_C^{\text{HB/H2}}$	$\tau_C^{\text{IP'}}$	$\tau_C^{\text{IP}}$	$\tau_C^{\text{cage}}$
RESP	0.61	0.53	0.77	1.38	0.38	60.87
NBO	0.55	0.66	3.38	3.80	0.23	—
SEN	0.28	0.32	0.60	1.14	0.52	101.08
0.7	0.43	0.39	0.61	1.09	0.39	32.06
0.9	0.95	0.75	1.02	1.78	0.37	113.27
$\text{H2}^0\text{C2}^0$	0.69	0.56	0.26	0.82	0.45	51.10
$\text{H2}^0\text{C2}^{0.19}$	0.66	0.59	0.23	1.14	0.55	58.18
$\text{H2}^{-0.19}\text{C2}^0$	0.68	0.55	0.09	1.30	0.57	93.18

<sup>a</sup> IP is with respect to the ring center of the imidazolium ring, IP' to the center of mass of the cation. All data were calculated at 373 K. Due to too slow dynamics, the missing data could not be calculated.

The effect of the charge sets on the hydrogen bond dynamics is shown in Table 4 and in Figure 7a,b. The details for calculating the correlation functions  $C$  and the relaxation times  $\tau$  as well as references can be found in the Supporting Information and in our previous publication.<sup>18</sup> For the continuous functions the hydrogen bond is not allowed to be broken, while for the intermittent it is allowed to be broken and to re-form. First of all, we analyzed the continuous hydrogen bond dynamics. For all charge sets we find the hydrogen bond dynamics at H2 to be the slowest compared to H4 and H5, except for the ones in which the charge on H2 is altered in order to change the hydrogen-bonding ability (cf. Table 4, column  $\tau_C^{\text{HB/H2}}$ ). Please note that due to the different hydrogen bond criteria we obtain different relaxation times as compared to our previous values.<sup>18</sup> Interestingly, the H4 and H5 dynamics are not equal, as reflected by the charges in Table 1 which result in sizable changes of the relaxation times for H4 and H5 in the different systems. This is also the reason for the reversed trend of these relaxation times for NBO and SEN as compared to RESP. If the total charge is altered by  $0.1$  e, the continuous dynamics are almost equally increased or decreased by  $0.2$ – $0.3$  ps, respectively. For the sets in which the C2–H2 charge is altered, only small changes for the continuous relaxation times  $\tau$  are observed at H4 and H5 and large changes are obviously found at H2. The relaxation time of H2 is decreased in each case, about a factor of 3 for the sets  $\text{H2}^0\text{C2}^0$  and  $\text{H2}^0\text{C2}^{0.19}$ , and almost about a factor of 10 for  $\text{H2}^{-0.19}\text{C2}^0$ .

Similar observations are made for the intermittent hydrogen bond dynamics, i.e., the functions for which the hydrogen bond is allowed to break and re-form again (cf. Figure 7a,b). The intermittent correlation function is very sensitive to small changes of the total charge, which is obvious from comparing the curves for the RESP and the total altered charges (black solid, dotted, and dashed curves in Figure 7). Strongly altered charges at the one hydrogen atom, namely H2, changes little at the other two ring hydrogen atoms (compare Figure 7b: blue and green curve). An exception is the intermittent hydrogen bond function for the charge set  $\text{H2}^{-0.19}\text{C2}^0$ . This function of H4 decays as slowly as for the 0.9 set—see red curve in Figure 7b. Obviously, the slope of the intermittent time correlation function of a particular hydrogen atom depends very strongly on its charge; see Figure 7a.

In Table 4 and in Figure 7d we show as well the data for the ion pair dynamics. As in our previous publication, we distinguish between the ion pair dynamics and the ion cage dynamics.



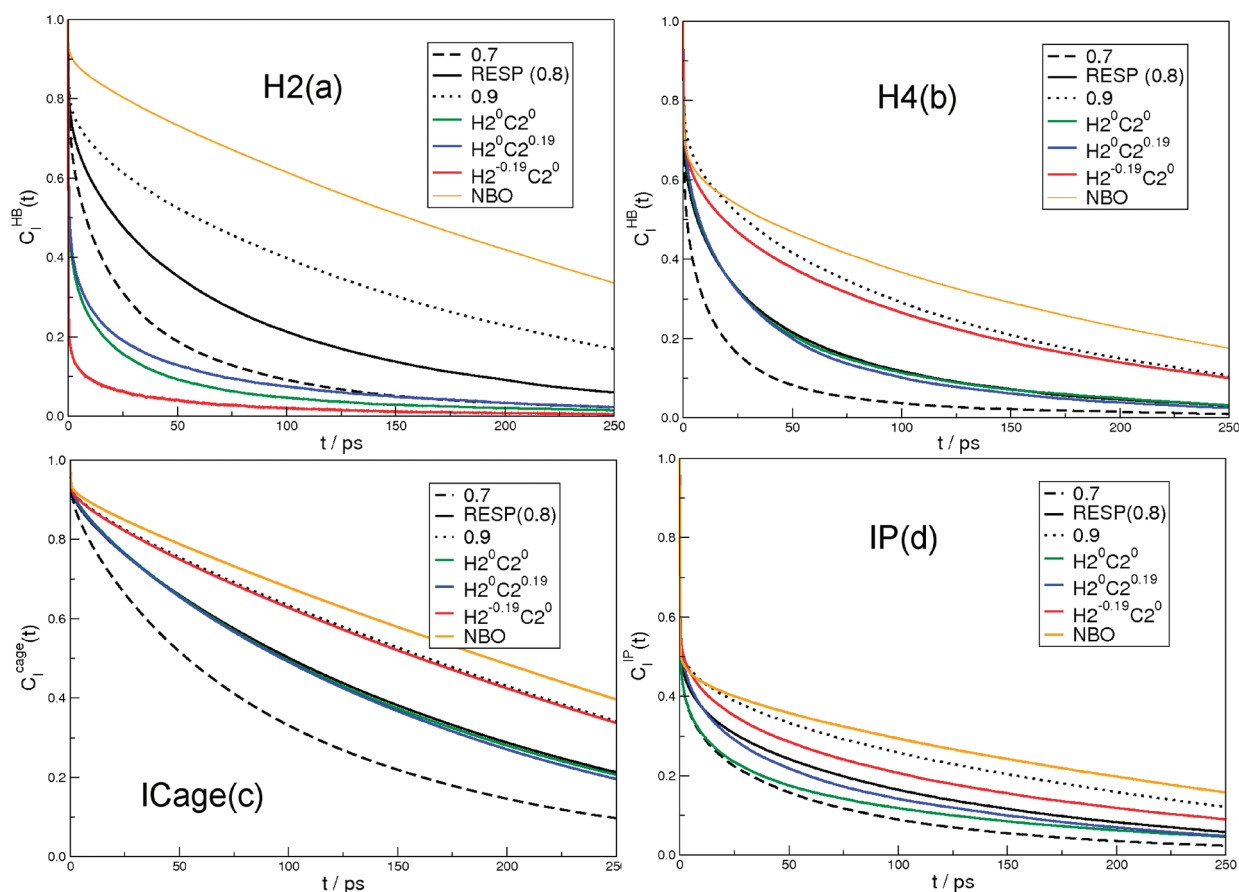


**Figure 7.**  $C_i^{\text{HB}}(t)$  for the H2 (a) and the H4 (b) hydrogen bond dynamics,  $C_i^{\text{cage}}(t)$  (c) and  $C_i^{\text{IP}}(t)$  (d) at 373 K. The SEN values are neglected for clarity.

The ion pair dynamics is *really* an ion pair dynamics, which means that we only counted the next neighboring anion at each time with respect to the ring center (called IP) or the center of mass (called IP') of one particular cation, respectively. We also calculated the functions previously termed ion cage dynamics (ICage). For the ion cage dynamics, all anions that are within an 800 pm sphere around the ring center are taken into account. Therefore, this definition describes the fact that an ion is surrounded by several counterions. An extended discussion of the differences can be found in section 4.4 of our previous publication.<sup>18</sup> The main conclusion was that in the presence of ion pairs the correlation times calculated according to both definitions should be in the same order of magnitude, which was not the case. We concluded that the ions exist in a fluctuating network and not as separated ion pairs. This discrepancy in the correlation times can be seen again by comparison of the last three rows in Table 4. Both ion pair dynamics are very fast, which means that the correlation times for the continuous ion pair dynamics are in the same order of magnitude ( $\tau_C^{\text{IP}}$ ) or only 1 order of magnitude larger ( $\tau_C^{\text{IP}'}$ ) than the correlation times for the hydrogen bond dynamics. In all cases  $\tau_C^{\text{IP}'}$  is larger than  $\tau_C^{\text{IP}}$ . This implies that an ion pair could be more stable when the next neighbor anion is situated in the proximity to the center of mass. One should keep in mind that the center of mass is, with respect to the imidazolium ring, shifted toward the butyl chain. Another important point is that the location of the center of mass depends on the conformation of the butyl chain and, therefore, it changes its position during the simulation time. Hence, several configurations contribute to this

correlation time. Concentrating on  $\tau_C^{\text{IP}'}$  for the RESP, the 0.7 and the 0.9 charge sets it behaves as expected (the higher the charge, the larger the correlation time); on the other hand, the  $\tau_C^{\text{IP}}$  is not influenced by total charge changes. A reason could be that the charge distribution on the imidazolium ring stays the same and due to the stiffness of the ring the relative orientation of the anion and the cation as well. Since there is no significant change in the SDFs depending on the total charge, too, one can assume that the stability of the on-top configuration (the anion is above or below the ring plane) is for this charge interval independent of the total ring charge. A weak or no hydrogen bond ability seems to improve the stability of the anion coordination next to the ring center; see  $\tau_C^{\text{IP}}$  of SEN,  $\text{H}_2^0\text{C}_2^0$ ,  $\text{H}_2^0\text{C}_2^{0.19}$ , and  $\text{H}_2^{-0.19}\text{C}_2^0$ . The charge distribution on the C2 and the H2 influences  $\tau_C^{\text{IP}'}$ ; see the last three rows of column four in table Table 4 but no trend can be observed. The correlation functions for the intermittent ion pair dynamics with respect to the center of mass can be seen from Figure 7d. The influence of the charge at H2 is more pronounced for the ion pair dynamics than for the ion cage dynamics, see below, but again an obvious trend could not be observed. The correlation times of the continuous motion of the ion cages are listed in the fourth column of Table 4 and the curves of their intermittent motions are depicted in Figure 7c. The ion cage dynamics provides for all charge sets the slowest motion. The total charge influences the ion cage dynamics as expected, the higher the charge the slower the dynamics. The charge on C2 has nearly no influence on this dynamics; see  $\tau_C^{\text{cage}}$  of RESP,  $\text{H}_2^0\text{C}_2^0$ , and  $\text{H}_2^0\text{C}_2^{0.19}$ . For the anti-hydrogen-bond situation  $\tau_C^{\text{cage}}$  is

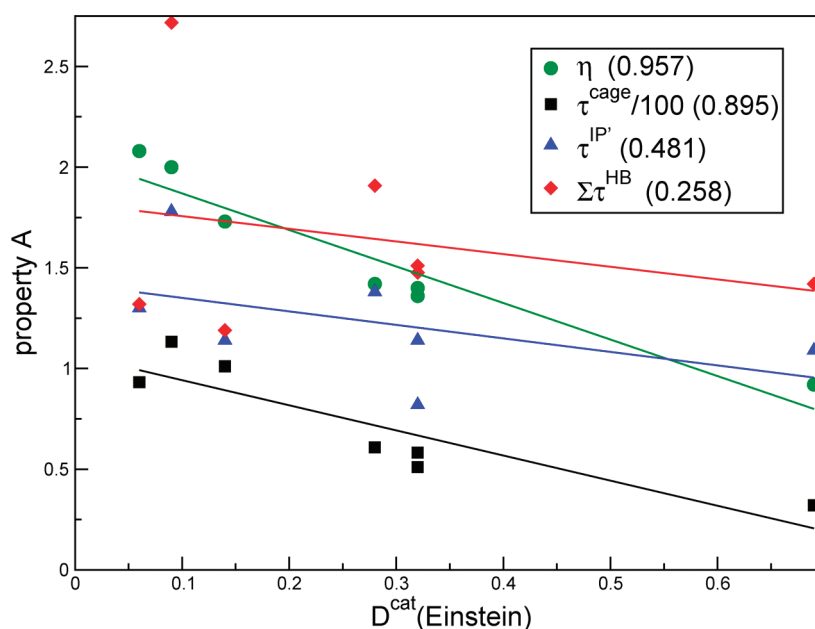


**Figure 8.** Correlation between diffusion coefficient and relaxation times of different motions.  $\Sigma\tau^{\text{HB}}$  indicates the sum over all three relaxation times of the ring hydrogen atoms.

nearly of the same size as for the highest charged systems, SEN and 0.9. The influence of the total charge on the intermittent time correlation function is rather large, whereas the hydrogen bond ability has little influence; see blue, black, and green curves in Figure 7c. Only in the extreme situation of an anti-hydrogen bond an increase in the slope is visible. In this case the ion cage dynamics is as slow as for the highest charged system; compare dotted black line and red line in Figure 7c. Conclusively, there seems to be no simple correlation between altered hydrogen bond and ion pair dynamics as well as ion cage dynamics. However, the influences are visible and can be rather large.

In order to see which quantity is most associated to the macroscopic dynamic properties, we show in Figure 8 a plot of viscosity and different dynamics as a function of the cation diffusion constant from Table 2. The numbers given in parentheses are the linear least-squares correlation coefficients.

Unsurprisingly, the viscosity and the diffusion coefficient are rather well correlated, although this is not necessarily the case. The best correlation of dynamics with the diffusion coefficient are found for the cage dynamics. Each ion pair and the hydrogen bond dynamics correlate rather weakly with the diffusion coefficient. This result indicates that the microscopic picture with regard to dynamics of an ionic liquid should be rather one of “ions dissolved in ions”<sup>43,44</sup> instead one of isolated ion pairs.<sup>45</sup>

## CONCLUSIONS

We carried out several simulations with different charge sets. The simulations, in which we altered the charges artificially, showed that structure and dynamics are differently affected by total charge of the ions and hydrogen-bonding ability of the ionic liquids. While the structure was largely influenced by hydrogen bonding, total charge alterations left the structure mostly unaffected. Different observations were made for the diffusion constant as well as the viscosity. While the total charges of the ions influenced the diffusion coefficients strongly, variations in the hydrogen bond did only manifest if drastic changes were

induced. As an example, increasing the strength of the hydrogen bond led to a reduced mobility. Similarly, decreasing the hydrogen bond strength to the point of simulating an “anti-hydrogen bond” resulted in the attraction of another cation in place of an anion. Naturally, the hydrogen bond dynamics was correlated to the changes of the charges at the particular hydrogen. Interestingly, the extreme situation of the anti-hydrogen bond at one hydrogen atom also affected the properties at the other ring hydrogen atoms. Much larger effects of changes at the one particular hydrogen atom were visible in the ion pair dynamics. This is probably due to the fact that often the next neighbor determining the ion pair was the one at the most acidic proton for which we altered the charges. There were also large effects in the ion cage dynamics (all next anion neighbors of one particular cation) if the total charge or the hydrogen bond situation was changed. From our simulations we observed that the cage dynamics was rather well correlated to the transport property. Therefore, we conclude that the picture of ionic liquids should be rather one of distributed ions than a picture of discrete ion pairs as was discussed previously. Although the correlation of the ion pair dynamics to the diffusion coefficient was weak and absent for the hydrogen bond, one should refrain from concluding that hydrogen bonding is unimportant for the behavior of the ionic liquid. First of all, this is not true for the structure, and the structure is responsible for the properties as solvent of the ionic liquid; together with the diffusion coefficient it will affect reactivity. Furthermore, there are secondary effects on the diffusion coefficient that we were able to show with our virtual experiment.

## ASSOCIATED CONTENT

**S Supporting Information.** Spatial distribution functions; diffusion coefficients; tables of diffusion coefficients; calculation of viscosity and table of viscosities; and hydrogen bond and ion pair dynamics. This material is available free of charge via the Internet at <http://pubs.acs.org>.



## AUTHOR INFORMATION

### Corresponding Author

\*E-mail: bkirchner@uni-leipzig.de.

## ACKNOWLEDGMENT

This work was supported by the DFG, in particular by the projects KI-768/4-1 and KI-768/4-2, KI-768/5-2, KI-768/5-3, KR 1138/20-3, and GI 355/6-1. Computer time from the RZ Leipzig and DEISA supercomputer center is gratefully acknowledged. Furthermore, support from the Deutsche Forschungsgemeinschaft within the Graduate School of Excellence Building with Molecules and Nanoobjects (BuildMoNa) is gratefully acknowledged.

## REFERENCES

- (1) Abdul-Sada, A. K.; Al-Juaied, S.; Greenway, A. M.; Hitchcock, P. B.; Howells, M. J.; Seddon, K. R.; Welton, T. *Struct. Chem.* **1990**, *1*, 391–394.
- (2) Wasserscheid, P.; Keim, W. *Angew. Chem., Int. Ed. Engl.* **2000**, *39*, 3772–3789.
- (3) Cremer, T.; Kolbeck, C.; Lovelock, K. R. J.; Paape, N.; Wölfel, R.; Schulz, P. S.; Wasserscheid, P.; Weber, H.; Thar, J.; Kirchner, B.; Maier, F.; Steinrück, H.-P. *Chem.—Eur. J.* **2010**, *16*, 9018–9033.
- (4) Kemptner, V.; Kirchner, B. *J. Mol. Struct. (THEOCHEM)* **2010**, *972*, 22–34.
- (5) Binnemans, K. *Chem. Rev.* **2005**, *105*, 4148–4204.
- (6) Lehmann, S. B. C.; Roatsch, M.; Schöppke, M.; Kirchner, B. *Phys. Chem. Chem. Phys.* **2010**, *12*, 7473–7486.
- (7) Hunt, P. A.; Kirchner, B.; Welton, T. *Chem.—Eur. J.* **2006**, *12*, 6762–6775.
- (8) Fumino, K.; Poppel, T.; Geppert-Rybczynska, M.; Zaitsau, D. H.; Lehmann, J. K.; Verevkin, S. P.; Köckerling, M.; Ludwig, R. *Phys. Chem. Chem. Phys.* **2011**, *13*, 14064–14075.
- (9) Bini, R.; Bortolini, O.; Chiappe, C.; Pieraccini, D.; Siciliano, T. *J. Phys. Chem. B* **2007**, *111*, 598–604.
- (10) Welton, T. *Chem. Rev.* **1999**, *99*, 2071–2083.
- (11) Crowhurst, L.; Mawdsley, P. R.; Perez-Arlandis, J. M.; Salter, P. A.; Welton, T. *Phys. Chem. Chem. Phys.* **2003**, *5*, 2790–2794.
- (12) Bodo, E.; Gontrani, L.; Triolo, A.; Caminiti, R. *2010*, *1*, 1095–1100.
- (13) Fumino, K.; Wulf, A.; Ludwig, R. *Angew. Chem., Int. Ed.* **2008**, *47*, 8731–8734.
- (14) Zahn, S.; Bruns, G.; Thar, J.; Kirchner, B. *Phys. Chem. Chem. Phys.* **2008**, *10*, 6921–6924.
- (15) Hunt, P. A. *J. Phys. Chem. B* **2007**, *111*, 4844–4853.
- (16) Endo, T.; Imanari, M.; Seki, H.; Nishikawa, K. *J. Phys. Chem. A* **2011**, *115*, 2999–3005.
- (17) Endo, T.; Kato, T.; Nishikawa, K. *J. Phys. Chem. B* **2010**, *114*, 9201–9208.
- (18) Kohagen, M.; Brehm, M.; Thar, J.; Zhao, W.; Müller-Plathe, F.; Kirchner, B. *J. Phys. Chem. B* **2011**, *115*, 693–702.
- (19) Reed, A. E.; Weinstock, R. B.; Weinhold, F. *J. Chem. Phys.* **1985**, *83*, 735–746.
- (20) Bayly, C. I.; Cieplak, P.; Cornell, W. D.; Kollman, P. A. *J. Phys. Chem.* **1993**, *97*, 10269–10280.
- (21) Davidson, E. *J. Chem. Phys.* **1967**, *46*, 3320.
- (22) Hardacre, C.; Holbrey, J. D.; McMath, S. E. J.; Bowron, D. T.; Soper, A. K. *J. Chem. Phys.* **2003**, *118*, 273–278.
- (23) Hardacre, C.; McMath, S. E. J.; Nieuwenhuyzen, M.; Bowron, D. T.; Soper, A. K. *J. Phys.: Condens. Matter* **2003**, *15*, S159–S166.
- (24) Embs, J. P.; Reichert, E.; Hempelmann, R. *Swiss Neutron News* **2007**, *32*, 4–9.
- (25) Thar, J.; Brehm, M.; Seitsonen, A. P.; Kirchner, B. *J. Phys. Chem. B* **2009**, *113*, 15129–15132.
- (26) Berendsen, H. J. C.; Postma, J. P. M.; van Gasteren, W. F.; DiNola, A.; Haak, J. K. *J. Chem. Phys.* **1984**, *81*, 3684.
- (27) Hess, B.; Kutzner, C.; van der Spoel, D.; Lindahl, E. *J. Chem. Theory Comput.* **2008**, *4*, 435–447.
- (28) Brehm, M.; Kirchner, B. *J. Chem. Inf. Model* **2011**, *51*, 2007–2023.
- (29) Sangoro, J. R.; Serghei, A.; Naumov, S.; Galvosas, P.; Kärger, J.; Wespe, C.; Bordusa, F.; Kremer, F. *Phys. Rev. E* **2008**, *77*, 051202.
- (30) Galvosas, P.; Stallmach, F.; Seiffert, G.; Kärger, J.; Kaes, U.; Majer, G. *J. Magn. Reson.* **2001**, *151*, 260.
- (31) Sangoro, J. R.; Iacob, C.; Naumov, S.; Valiullin, R.; Rexhausen, H.; Hunger, J.; Buchner, R.; Strehmel, V.; Kärger, J.; Kremer, F. *Soft Matter* **2011**, *7*, 1678–1681.
- (32) Kremer, F.; Schönhals, A., Eds. *Broadband Dielectric Spectroscopy*; Springer: Berlin, 2003.
- (33) Youngs, T. G. A.; Hardacre, C. *ChemPhysChem* **2008**, *9*, 1548–1558.
- (34) Umecky, T.; Kanakubo, M.; Ikushima, Y. *Fluid Phase Equilib.* **2005**, *228–229*, 329–333.
- (35) Lynden-Bell, R. M.; Youngs, T. G. A. *J. Phys.: Condens. Matter* **2009**, *21*, 424120.
- (36) Sangoro, J.; Iacob, C.; Serghei, A.; Naumov, S.; Galvosas, P.; Kaerger, J.; Wespe, C.; Bordusa, F.; Stoppa, A.; Hunger, J.; Buchner, R.; Kremer, F. *J. Chem. Phys.* **2008**, *128*, 214509.
- (37) Yan, T.; Burnham, C. J.; Pópolo, M. G. D.; Voth, G. A. *J. Phys. Chem. B* **2004**, *108*, 11877–11881.
- (38) Borodin, O. *J. Phys. Chem. B* **2009**, *113*, 12353–12357.
- (39) Maginn, E. J. *J. Phys.: Condens. Matter* **2009**, *21*, 373101.
- (40) Kim, K.; Shin, B.; Lee, H. *Korean J. Chem. Eng.* **2004**, *21*, 1010–1014.
- (41) Grishina, E. P.; Kudrayakova, N. O. *Colloid Chem. Electrochem.* **2010**, *84*, 589–593.
- (42) Kirchner, B. *Top. Curr. Chem.* **2010**, *290*, 213–262.
- (43) Lui, M. Y.; Crowhurst, L.; Hallett, J. P.; Hunt, P. A.; Niedermeyer, H.; Welton, T. *Chem. Sci.* **2011**, *2*, 1491–1496.
- (44) Schröder, C. *J. Chem. Phys.* **2011**, *135*, 024502.
- (45) Zhao, W.; Leroy, F.; Heggen, B.; Zahn, S.; Kirchner, B.; Balasubramanian, S.; Müller-Plathe, F. *J. Am. Chem. Soc.* **2009**, *131*, 15825–15833.